AIP | Journal of Applied Physics

Experimental characterization and modeling of a nanofiber-based selective emitter for thermophotovoltaic energy conversion: The effect of optical properties

M. T. Aljarrah, R. Wang, E. A. Evans, C. B. Clemons, and G. W. Young

Citation: Journal of Applied Physics **109**, 034306 (2011); doi: 10.1063/1.3524567
View online: http://dx.doi.org/10.1063/1.3524567
View Table of Contents: http://scitation.aip.org/content/aip/journal/jap/109/3?ver=pdfcov
Published by the AIP Publishing

Experimental characterization and modeling of a nanofiber-based selective emitter for thermophotovoltaic energy conversion: The effect of optical properties

M. T. Aljarrah,[1] R. Wang,[1] E. A. Evans,[1,a)] C. B. Clemons,[2] and G. W. Young[2]
[1]*Department of Chemical and Biomolecular Engineering, University of Akron, Akron, Ohio 44325-3906, USA*
[2]*Department of Theoretical and Applied Mathematics, University of Akron, Akron, Ohio 44325-4002, USA*

(Received 23 April 2010; accepted 1 November 2010; published online 4 February 2011)

Aluminum oxide nanofibers doped with erbium oxide have been synthesized by calcining polymer fibers made by the electrospinning technique using a mixture of aluminum acetate, erbium acetate and polyvinylpyrrolidone dissolved in ethanol. The resulting ceramic fibers are used to fabricate a free-standing selective emitter. The general equation of radiation transfer coupled with experimentally measured optical properties is used to model the net radiation obtained from these structures. It has been found that the index of refraction and the extinction coefficient are direct functions of the erbia doping level in the fibers. The fibers radiated in a selective manner at $\sim$1.53 μm with an efficiency of about 90%. For a fiber film on a substrate, the effect of film thickness, extinction coefficient and substrate emissivity on the overall emitter emissivity is also investigated in this study. Results show that the emissivity of the film increases as the thickness of the film increases up to a maximum value, after which increasing the film thickness had no effect on emissivity. Furthermore, it has been found that the substrate emissivity increases the amount of off-band radiation. This effect can be mitigated by controlling the film thickness. © *2011 American Institute of Physics*. [doi:10.1063/1.3524567]

I. INTRODUCTION

In thermophotovoltaic (TPV) technology, infrared radiation from a hot emitter is converted into electricity by utilizing the photovoltaic (PV) effect. A conventional TPV system consists of a heat source, an emitter and a photo diode (semiconductor p/n junction). In contrast to solar electric generators which use solar radiation (mainly in the visible range), a TPV radiator emits mainly in the infrared range and can be heated using many heating sources. The emitter (radiator) can be a broadband or a narrowband emitter. Since photocells can only convert radiation in certain wavelength ranges, a filter has to be used to achieve the spectral match between the radiator and the PV cell when a broadband emitter is used. Any radiation incident on the PV cell that cannot be converted into electricity will increase the temperature of the cell and, therefore, decrease its efficiency[1] (defined as electrical energy generated/radiation incident on the cell).

Selective emitters which radiate most of their energy in a narrow wavelength range usable by the PV cell can also be used as radiators. Using a selective emitter increases the efficiency of the PV cell[2] and minimizes the need for optical control or an additional cooling system. In addition to the spectral match with the PV cell, the emitter should be chemically and mechanically stable. Rare earth oxides were the first materials to be used as selective emitters for TPV applications.[3] The first emission data for rare earth oxide published by Guazzoni[4] used specimens of rare earth powders pressed into thin disks. Since then, rare earth oxides have been used in different forms to fabricate selective emitters that can meet the functional and the thermostructural challenges of TPV systems.[5]

Selective emitters in the fibrous form provide a functional and mechanical advantage over other types of emitters and were suggested by many researchers to overcome the poor thermal shock resistance problem in these other emitters.[6] Fibrous media have high efficiency in suppressing radiation energy transfer by absorption or scattering[7] which makes them a good candidate for high temperature insulation and other applications that involve high temperatures. In recent years, electrospun ceramic fibers doped with rare earth ions were used to fabricate a selective emitter for thermphotovoltaic applications.[8,9] Electrospun ceramic fibers are porous in nature, have diameters in the submicron range, and have a very high surface to volume ratio.

The subject of radiation transfer through fibrous media is extensively studied in the literature. An excellent review of the models that are used to calculate radiation energy transport in fibrous media is given by Lee and Cunnington.[10] A one-dimensional (1D) mathematical model for thin film selective emitters was developed by Chubb and Lowe[11] They found that using a substrate with low emittance ($<$0.05) is essential to obtain high efficiency emitters. The effect of temperature gradients on the emittance of thick film selective emitters was also studied by Chubb and co-workers.[12] Since ceramic materials have very low thermal conductivity, temperature gradients are expected to form (as high as 200 K in 1 mm thick samples[12,13]). Temperature gradients across the

a)Electronic mail: evanse@uakron.edu.

section of the emitter can greatly reduce its emission; the colder regions of the emitter can absorb the radiation from the hotter regions.

Previous work on the modeling of thin film selective emitters has led to three important conclusions: (i) Only substrates with very low emissivity can be used as a support for the thin film emitters. Substrates with high emissivity decrease the efficiency of the emitter by increasing the amount of off-band radiation.[13] (ii) The temperature gradient inside the film leads to a decrease in the radiation from the emitter.[12] (iii) The effect of scattering can be neglected for single crystal materials, but not for multigrain materials.[5]

In this study, a self-supporting selective emitter is fabricated using electrospun aluminum oxide fibers doped with erbium oxide. Optical properties of the fabricated emitters including the extinction coefficient, the index of refraction and the surface reflectivity are calculated from experimentally measured values of reflectance and transmittance at room temperature. The optical properties are input to a 1D model to predict the radiation intensity from these emitters. The results obtained from the model are compared with the experimental results. A satisfactory agreement is found. The model is then used to quantify the effect of film thickness, extinction coefficient, and substrate emissivity on film emissivity and suggest designs that are more efficient without the need for difficult emission measurements.

II. THEORETICAL BACKGROUND

For a beam of light traveling through an arbitrary volume element with thickness S in a radiatively participating medium, the intensity of the beam I_λ, will change due to internal emission, absorption and scattering. The general form of the equation of radiation transfer in a medium can be written as follows, assuming that the time dependence of the radiative intensity is neglected,[14]

$$\frac{dI_\lambda}{ds} = -\kappa_\lambda I_\lambda - \sigma_\lambda I_\lambda + \kappa_\lambda I_{b\lambda} + \frac{\sigma_\lambda}{4\pi}\int_0^{4\pi} I_\lambda(\hat{s}_i)\Phi_\lambda(\hat{s}_i,s)d\omega. \tag{1}$$

In Eq. (1), κ_λ is the absorption coefficient, σ_λ is the scattering coefficient, Φ_λ is the phase function and ω is the solid angle. The left hand side is the change in radiation intensity as it travels along the direction s through the medium. The first two terms on the right hand side are the attenuation due to absorption and scattering, respectively. The third term represents the increase in intensity by internal emission and finally the fourth term represents the increase in intensity due to the rescattering of the scattered radiation into the original direction of the radiation transfer.

The net attenuation due to scattering and absorption is known as extinction. Assuming that both absorption and scattering are significant, we define the extinction coefficient as

$$\beta_\lambda = \sigma_\lambda + \kappa_\lambda, \tag{2}$$

where σ_λ and κ_λ are the scattering and absorption coefficients, respectively. The absorption coefficient is a strong function of the wavelength (λ). The scattering coefficient is a function of wavelength, coherence, and polarization of the incident beam, as well as the physical properties of the medium such as particle size, shape, and type.[15] The optical depth based on the total extinction coefficient is

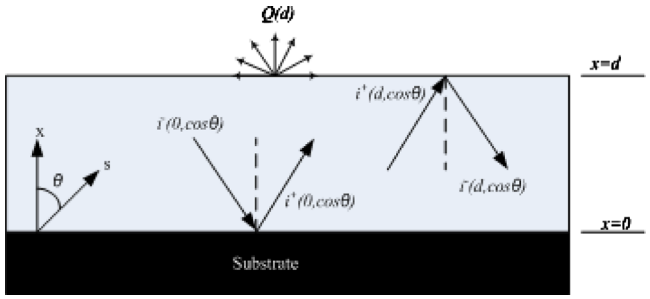

FIG. 1. (Color online) Thin film selective emitter on a blackbody substrate (Ref. 17).

$$\tau_\lambda = \int_0^s \beta_\lambda dS. \tag{3}$$

By using the definition of the extinction coefficient in Eq. (2), we write the equation of radiation transfer in the form

$$\frac{dI_\lambda}{ds} = -\beta_\lambda I_\lambda + \kappa_\lambda I_{b\lambda} + \frac{\sigma_\lambda}{4\pi}\int_0^{4\pi} I_\lambda(\hat{s}_i)\Phi_\lambda(\hat{s}_i,s)d\omega, \tag{4}$$

where $I_{b\lambda}$ is the intensity of blackbody radiation and $\Phi_\lambda(\hat{s}_i,s)$ is the phase function which represents the probability of the scattered radiation from any direction $\hat{s}_i$ to be "rescattered" back in the s direction. For isotropic scattering, where radiation is scattered equally in all directions, the phase function $\Phi_\lambda(\hat{s}_i,s)$ equals 1. To account for light rescattered from all directions, the incident intensity is integrated over the entire range of solid angle ω. If we define the *albedo of scattering*, Ω_λ, as the ratio of the scattering coefficient to the extinction coefficient, and make a change from the variable s to the variable τ_λ [defined in Eq. (3)], the equation of radiation transfer can be written as

$$\frac{dI_\lambda}{d\tau_\lambda} + I_\lambda = S_\lambda(\tau_\lambda,s), \tag{5}$$

where $S_\lambda(\tau_\lambda,s)$ is the source function defined as follows:

$$S_\lambda(\tau_\lambda,s) = (1-\Omega_\lambda)I_{b\lambda} + \frac{\Omega_\lambda}{4\pi}\int_{4\pi} I_\lambda(\hat{s}_i)\Phi_\lambda(\hat{s}_i,s)d\omega. \tag{6}$$

This compact form of the equation of radiation transfer [Eq. (5)] can be solved using an integration factor of the form e^{τ_λ} to find

$$I_\lambda(\tau_\lambda) = I_\lambda(0)e^{-\tau_\lambda} + \int_0^{\tau_\lambda} S_\lambda(\tau'_\lambda,s)e^{-(\tau_\lambda-\tau'_\lambda)}d\tau'_\lambda. \tag{7}$$

For a plane layer of emitting, absorbing and scattering material as shown in Fig. 1, assuming that the properties of the layer will change only in the x-direction, the net radiation flux $Q(d)$ from the surface of the film with thickness d can be found by writing general expressions for the positive and negative radiation intensities i^+ and i^-.[16]

Since the properties of the medium change only in one direction (the x-direction in this case), the optical depth defined in Eq. (3) can be redefined along the x-direction

$$\tau_\lambda(s) = \int_0^s \beta_\lambda(s^*)ds^* = \int_0^{x/\cos\theta} \beta_\lambda\left(\frac{x^*}{\cos\theta}\right)d\left(\frac{x^*}{\cos\theta}\right)$$

$$= \frac{1}{\cos\theta}\int_0^x \beta_\lambda(x^*)dx^* = \tau_\lambda(x)/\cos\theta. \quad (8)$$

Using the transformation in Eq. (8), the radiation intensity in the positive and negative x-direction shown in Fig. 1 (Ref. 17) can be written as

$$i_\lambda^+(\tau_\lambda,\cos\theta) = i_\lambda^+[\tau_\lambda(0),\cos\theta]\exp\left(\frac{-\tau_\lambda}{\cos\theta}\right) + \int_0^{\tau_\lambda} S_\lambda(\tau'_\lambda,\cos\theta)\exp\left[\frac{-(\tau_\lambda-\tau'_\lambda)}{\cos\theta}\right]\frac{d\tau'_\lambda}{\cos\theta},$$

$$0 \le \cos\theta \le 1, \quad (9)$$

$$i_\lambda^-(\tau_\lambda,\cos\theta) = i_\lambda^-[\tau_\lambda(d),\cos\theta]\exp\left(\frac{\tau_\lambda(d)-\tau_\lambda}{\cos\theta}\right) - \int_0^{\tau_{\lambda d}} S_\lambda(\tau'_\lambda,\cos\theta)\exp\left[\frac{-(\tau'_\lambda-\tau_\lambda)}{\cos\theta}\right]\frac{d\tau'_\lambda}{\cos\theta},$$

$$-1 \le \cos\theta \le 0. \quad (10)$$

Equations (9) and (10) can be solved simultaneously to obtain the radiation intensities i_λ^+ and i_λ^-.

A. Solution of the model

An analytical solution to the general equation of radiation transfer is only available in the case of isotropic scattering.[18] However, in the case where scattering can be neglected, the source function is reduced to blackbody radiation which is a function of temperature only. For a detailed mathematical analysis of the phenomena of radiation transfer in a participating medium, the reader is referred to the text published by Siegel and Howell;[19] Chubb also published an excellent book on fundamentals of TPV energy conversion which included his mathematical modeling work for thin film selective emitters.[18] For more methods to solve the equation of radiation transfer such as the Monte Carlo method or the method of discrete ordinates the reader is referred to the text by Modest.[17]

In this study, the analytical solution given by Chubb and co-workers will be used to calculate the emissivity of the fabricated emitters.[12,15,20–22] The emissivity of a thin film selective emitter as illustrated in Fig. 1 above can be calculated from

$$\varepsilon(\lambda) = \frac{Q(d)}{e_{BB}(\lambda,T)}, \quad (11)$$

where $e_{BB}(\lambda,T)$ is the power radiated from a blackbody at the same temperature of the film (T) and can be calculated using Planck's equation. $Q(d)$ is the power emitted at the surface of the film and can be calculated from

$$Q(d) = 2\pi\int_{\theta=0}^{\theta=\theta_M}[i_\lambda^+(\tau_{\lambda d},\cos\theta) - i_\lambda^-(\tau_{\lambda d},\cos\theta)]\cos\theta\sin\theta d\theta. \quad (12)$$

Since the index of refraction of the film is higher than that of the surrounding medium (air or vacuum), total reflection at the film interface is expected to take place according to Snell's law and hence, the upper limit of the integration in Eq. (12) is the total reflection angle θ_M defined according to Snell's law as

$$\sin\theta_M = \frac{n_0}{n_f}, \quad (13)$$

where n_0 and n_f are the indices of refraction for the surrounding (air or vacuum) and the film, respectively. Before solving Eqs. (9) and (10) for i_λ^+ and i_λ^-, the source function needs to be defined. In the simplest case where the effect on the source of scattering is completely neglected, the source function is reduced to the blackbody intensity as shown in Eq. (6). When $\Omega_\lambda \to 0$, the source function $S(\tau_\lambda,\hat{s}) \to I_{b\lambda}$ and the integrations in Eqs. (9) and (10) can be carried out. Solving Eqs. (9) and (10) for i_λ^+ and i_λ^- and then substituting in Eqs. (11) and (12), we find the emissivity is given by

$$\varepsilon = \frac{n_f^2(1-\rho_{\lambda 0})}{D}\left\{2B\left\{\frac{\varepsilon_s(1-\rho_{\lambda s})}{n_{\lambda s}^2} + \rho_{\lambda s}[1-2E_3(\tau_{\lambda d})]\right\} + A[1-2E_3(\tau_{\lambda d})] - (\cos\theta_M)^2 D\left[1-2E_3\left(\frac{\tau_{\lambda d}}{\cos\theta_M}\right)\right]\right\}, \quad (14)$$

where

$$A = 1 - 4\rho_{\lambda 0}\rho_{\lambda s}(\cos\theta_M)^2 E_3(\tau_{\lambda d})E_3\left(\frac{\tau_{\lambda d}}{\cos\theta_M}\right), \quad (15)$$

$$B = E_3(\tau_{\lambda d}) - (\cos\theta_M)^2 E_3\left(\frac{\tau_{\lambda d}}{\cos\theta_M}\right), \quad (16)$$

$$D = 1 - 4\rho_{\lambda 0}\rho_{\lambda s}[E_3(\tau_{\lambda d})]^2, \quad (17)$$

and E_n is the general exponential integral defined as

$$E_n(x) = \int_0^1 \upsilon^{n-2}\exp\left(\frac{-x}{\upsilon}\right)d\upsilon, \quad (18)$$

and $\rho_{\lambda 0}$ and $\rho_{\lambda s}$ are the reflectivities at the film/air and film/substrate interfaces, respectively.

B. Extinction coefficient and other optical properties

Several parameters are needed in the set of Eqs. (14)–(18). These include the reflectivities at the film/substrate and film/air interfaces, the indices of refraction for the film, the substrate, and the surrounding (air/vacuum), and most importantly, the extinction coefficient of the film. These parameters are calculated using the net radiation method proposed by Siegel and Howell[19] using experimentally measured values of reflection, transmission, and absorption. A schematic illustration of this method is shown in Fig. 2 for a

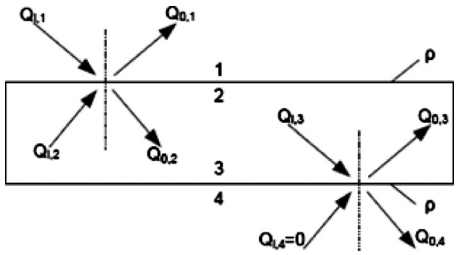

FIG. 2. Net radiation method applied on a plane layer geometry (Ref. 18).

partially transmitting layer. According to this method, the outgoing radiation flux Q at each interface can be written in terms of the incident fluxes at that interface. For a unity incident flux on surface 1 ($Q_{i,1}=1$), the following equations can be written for the outgoing radiation fluxes at interfaces 1, 2, 3, and 4 shown in Fig. 2,

$$Q_{0,1} = \rho\left[1 + \frac{(1-\rho)^2\tau^2}{1-\rho^2\tau^2}\right], \tag{19}$$

$$Q_{0,2} = \left[\frac{(1-\rho)}{1-\rho^2\tau^2}\right], \tag{20}$$

$$Q_{0,3} = \rho\tau\frac{(1-\rho)}{1-\rho^2\tau^2}, \tag{21}$$

$$Q_{0,4} = \left[\frac{(1-\rho)^2\tau}{1-\rho^2\tau^2}\right]. \tag{22}$$

The parts of the incident beam that are reflected and transmitted by the medium are

$$R_\lambda = Q_{0,1}, \tag{23}$$

$$T_\lambda = Q_{0,4}, \tag{24}$$

and the fraction absorbed by the medium is

$$A = (Q_{0,2} + Q_{0,3})(1-\tau), \tag{25}$$

where ρ and τ are the reflectance at the surface and the internal transmittance (transmissivity of the layer), respectively. If we assume that the material behaves according to the Beer–Lambert law and the reflectivity is the same at both surfaces, the internal transmittance τ can be written as[12]

$$\tau = e^{-\beta_\lambda d} = \frac{1}{2}\left\{\sqrt{\left[\frac{T_\lambda^2 - (1-R_\lambda)^2}{T_\lambda}\right]^2 + 4} + \frac{1}{T_\lambda}[T_\lambda^2 - (1-R_\lambda)^2]\right\}. \tag{26}$$

According to Eq. (26) the extinction coefficient β_λ can be calculated from measured values of reflectance and transmittance. The index of refraction is calculated according to Eq. (27) for incident angles larger than the total reflection angle defined by Snell's law

$$\rho_{\lambda 0} = \left(\frac{n_f - n_0}{n_f + n_0}\right)^2, \tag{27}$$

where n_0 can be taken as 1.

III. FIBER FABRICATION

Sheets of aluminum oxide fibers are fabricated from fibers produced by the electrospinning technique. Electrospinning is a simple method by which ultrathin polymer fibers (in the submicron range, one or two orders of magnitude smaller diameter than fibers produced by extrusion[23]) can be produced. Polymer fibers spun using a solution loaded with ceramic precursors can be further processed to form ceramic and composite fibers. Many ceramic fibers were successfully produced from electrospun fibers including Al_2O_3,[24] SiO_2,[25] YSZ,[26] PdO,[27] and TiO_2.[28] An excellent review on electrospinning of ceramic nanofibers is published by Wolfgang *et al.*[29]

In this study, polyvinylpyrrolidone (PVP) solution is made by mixing 3 g of PVP powder (Sigma-Aldrich, Mwt: 1 300 000, CAS: 9003-39-8) with 30 ml of absolute ethanol. The solution is left at room temperature to homogenize for 24 h. Aluminum acetate (CAS: 7360-44-3, Strem Chemicals) is used as a chemical precursor for aluminum oxide. 20 g of aluminum acetate is dissolved in 40 ml of water and 52 ml of ethanol. The solution is mixed on a magnetic mixer until the aluminum acetate is completely dissolved. Erbium acetate [Erbium (III) acetate hydrate, 99.9%, CAS: 15280-57-6] is then added. The two solutions are mixed together in a 1:1 volume ratio and left for 24 h at room temperature before electrospinning.

Fibers are produced by applying a large voltage difference between a solution, normally fed through a syringe needle, and a collecting plate. In this work, 3 ml of the solution is loaded into a syringe and connected to the needle using Teflon tubing. The syringe is placed in a syringe pump. The solution is pumped at a flow rate of 5 μL/min. The voltage is set to 20 kV and the distance between the tip of the needle and the collecting sheet is approximately 20 cm. The spun fibers are collected on a rotating drum wrapped with aluminum foil and set to rotate at a rate of 50 rpm using a motor and controller. The fibers are then calcined in a tube furnace at 700 °C. The heating rate is approximately 5 °C/min and the fibers are kept at the target temperature for 2 h and then cooled to room temperature.

IV. RESULTS AND DISCUSSION

Our goal in this study is to create a model that can be used to guide the design of efficient selective emitters based on electrospun ceramic nanofibers doped with rare earth oxide. This model will serve as a basis for our extended modeling work that will take into account the geometry of the selective emitter and the spatial distribution of the emitting material as shown in the second part of this study.[30] The parameters needed to solve the set of Eqs. (11)–(17) are the extinction coefficient, the index of refraction and the surface reflectivity. These parameters are calculated as a function of wavelength and erbium oxide concentration in the fibers using experimentally measured data of reflection and transmission. Furthermore, the model is validated by comparing the theoretical data with experimental data of radiation intensity obtained from our samples. The experimental details of the validation method are given in Sec. IV D.

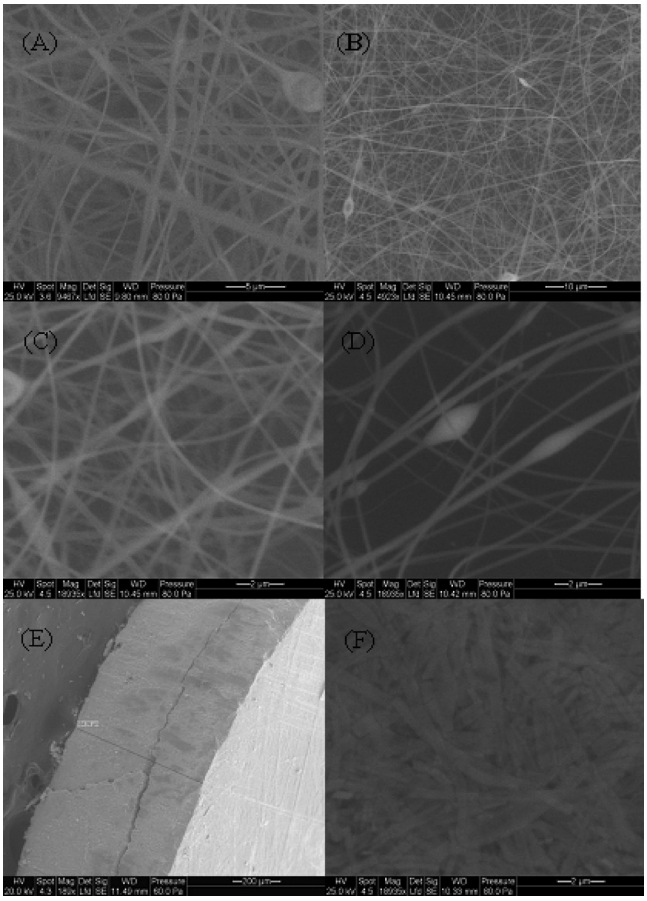

FIG. 3. SEM images of erbia doped alumina at different erbium oxide concentration. (a) 1%, (b) 5%, (c) 10%, and (d) 15%. Samples annealed at 700 °C. [(e) and (f)] Side and top view of pressed pellet.

A. Morphology study of the emitter media

Scanning electron microscopy (SEM) images of the erbia doped alumina fibers fabricated in this study are shown in Fig. 3. The fibers are in the submicron range (<1 μm in average) and have a circular cross-section. Beading of the fibers is noticed in the SEM images. Bead formation can be controlled by controlling the surface tension of the solution, the charge density, and the applied voltage.[31] Tripatanasuwan *et al.*[32] studied the bead formation process in polymer fibers made using the electrospinning technique and found that beads form when the jet diameter is very thin. The bead diameter and the spacing between the beads were influenced by the relative humidity during electrospinning. The bead diameter increased with increasing humidity whereas the spacing between the beads and the bead lengths decreased with increasing relative humidity. Controlling bead formation is beyond the scope of this study.

The calcined fibers are brittle and difficult to handle. Moreover, emissivity measurements of the fibers in their loose form are highly irreproducible. In order to make a regular sample shape that can be easily handled and reproduced, fiber pellets are made from the electrospun fibers. The calcined fibers are pressed into pellets using a mechanical press at 2500 lb of pressure. No filler or binder of any kind is used. The pellets are 6 mm in diameter and the thickness range is 150–900 μm depending on the amount of fibers used. SEM images of the pressed pellet are shown in Fig. 3. The fibers retained their shape after pressing.

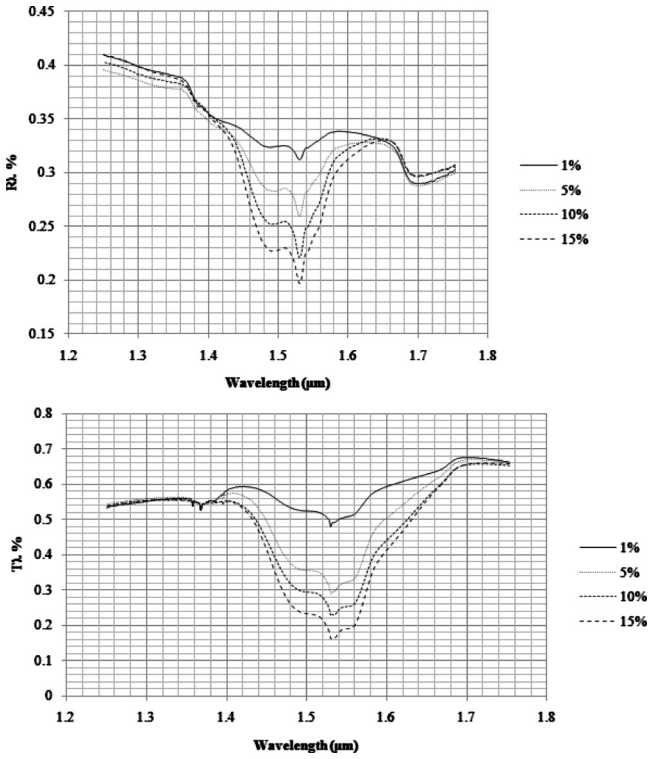

FIG. 4. Reflectance and transmittance measurements of erbia doped alumina fibers for different erbia loading from 1% to 15% Er/Al atomic ratio in the NIR range.

B. Optical properties

The optical properties of erbium oxide-doped alumina fiber samples with different erbia concentration are calculated using values of reflectance and transmittance according to Eqs. (26) and (27). The measurements are performed using a Bruker IFS 66 v/s spectrometer in the near-IR (NIR) range. The measurements are performed under vacuum (typically 3 mbar) with a resolution of 4 cm^{-1}. A tungsten source, CaF_2 beamsplitter, and thermoelectrically cooled InGaAs detector are used. The wavelength range is from 5800–8000 cm^{-1}. Reflectance measurements are made using an auto seagull setup. All measurements are made at room temperature.

Figure 4 shows the spectral reflectance and transmittance measurements. The erbium signature peak is shown in both curves at ~1.53 μm. One goal of this study is to track the changes in the NIR signature bands of Er^{3+} centered approximately at 1.53 μm with increasing concentration of Er^{3+}. The distinctive IR features of lanthanides result from the localization of their $4f$ electrons.[2] In the case of Er, the main peak at 1.53 μm is a result of the transitions from the $^4I_{15/2}$ state to the $^4I_{13/2}$.[8]

The values of reflectance and transmittance at 1.53 μm can be used to calculate the index of refraction and the extinction coefficient of the sample according to Eqs. (26) and (27). Figure 5 shows the calculated values of the extinction coefficient of the samples using Eq. (26). The extinction co-

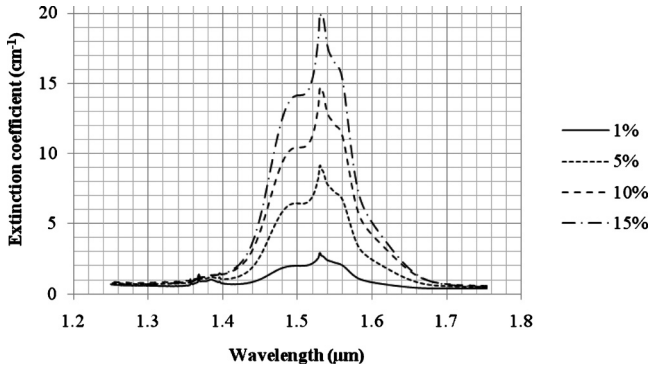

FIG. 5. Extinction coefficient as function of wavelength calculated using Eq. (26) and the data in Fig. 4 for different erbia loadings from 1% to 15% Er/Al atomic ratios.

efficient has a direct effect on the emissivity and the total useful power radiated from the samples. The higher the value of the extinction coefficient inside the desired wavelength range, the higher the emissivity of the sample and the higher the useful power radiated from it. Chubb[22] reported values of about 40, 60, 80, and 100 cm^{-1} for 30%, 36%, 54%, and 50% erbium/aluminum atomic ratio in erbia doped yttrium aluminum garnet. In this study, a 20 cm^{-1} extinction coefficient is achieved for a 15% Er/Al atomic ratio.

Figure 6 shows the values of the index of refraction in the NIR range for the fabricated samples. The values are calculated using Eq. (27) and the reflectance data in Fig. 4. The index of refraction is a strong function of wavelength. The wavelength dependence of the index of refraction is the same as that for the reflectance measurements. The index of refraction of pure erbium oxide is 1.9. Chubb and co-workers reported values of about 2.3 at a wavelength ~1500 nm for a selective emitter made of erbia reinforced alumina. In this study, values of the index of refraction range from 3.5 to 2.2 depending on the erbium oxide concentration inside the fiber.

C. Modeling results

The optical properties of the samples calculated in the previous section are used in the mathematical model to calculate the emissivity and total radiated power. We use Eq. (14) to find the variation in the film emittance with the film thickness for different values of the extinction coefficient.

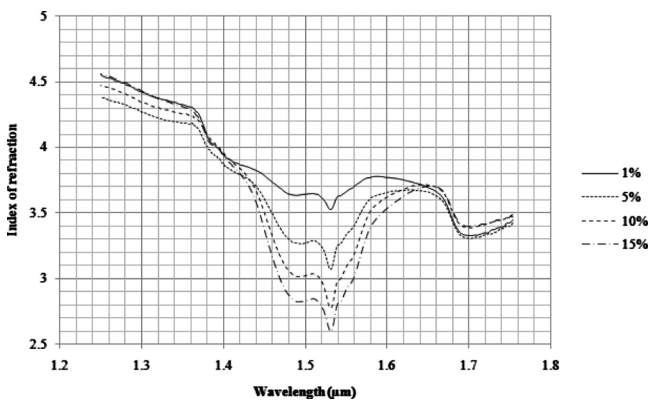

FIG. 6. Index of refraction for erbia doped alumina fibers for various concentration of erbium oxide calculated using Eq. (27) and the data in Fig. 4.

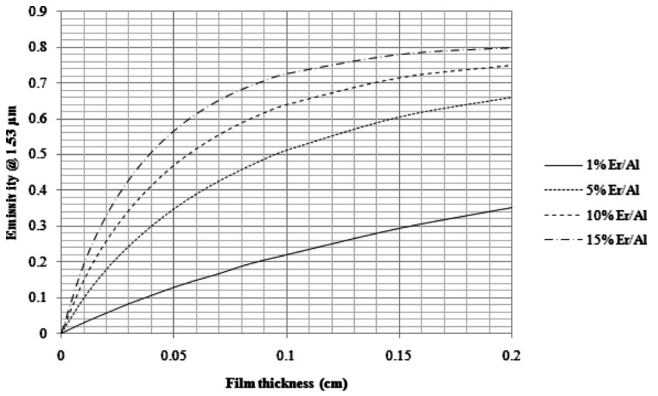

FIG. 7. Emissivity calculated from Eq. (14) of a thin film (at 1.53 μm) as a function of the film thickness for different Er/Al atomic ratios. The extinction coefficient values are taken from Fig. 5. These values at $\lambda = 1.53$ μm are 2.8 cm^{-1}, 9.1 cm^{-1}, 14.7 cm^{-1}, and 20.0 cm^{-1} for 1%, 5%, 10%, and 15% Er/Al respectively.

The results are shown in Fig. 7. The calculations are performed for a free-standing selective emitter (no substrate is used, emissivity of the substrate=0). The thickness of the film required to obtain high emissivity increases with a decrease in extinction coefficient of the film.

Evidently from Fig. 7, the same emissivity may be obtained for different extinction coefficient values by changing the physical thickness of the film. From Eq. (14), the emissivity of the film is a function of optical depth which is the product of the extinction coefficient and the thickness of the film which means that the same emissivity can be obtained by changing either one of them. This result compares very well with those reported by Krishna *et al.*[33]

Knowing that the extinction coefficient is the summation of both the absorption and the scattering coefficient, one could predict the parameters that affect it. For the erbium-oxide doped fibrous emitter fabricated in this study, the absorption coefficient is a direct function of the erbium-oxide concentration as shown in Fig. 5. The scattering coefficient is a function of the physical parameters of the emitter, such as the fiber diameter, the crystal size, the porosity of the emitter, the refractive index, etc.

D. Model validation

To validate the model, we compare emission measurements to model calculations. The emissivity of the samples is measured using a novel thermal emission setup as shown in Fig. 8. The sample is placed in a quartz holder which is placed inside an L-shaped quartz tube. A heat gun is used to blow hot air inside the tube to heat the sample to a temperature of 773 K for emission measurements. The sample temperature is measured using a thermocouple placed in front of the sample holder. It is assumed that the temperature of the sample is the same as the temperature of the hot air stream after allowing sufficient time to reach thermal equilibrium. We believe that this assumption is valid since the sample volume is very small and it has a highly porous structure. The porosity of the sample is 54.82% (V_{void}/V_{total}). The temperature reading was stable in a ± 3 °C range during measurements. The sample holder is located in the focal point of

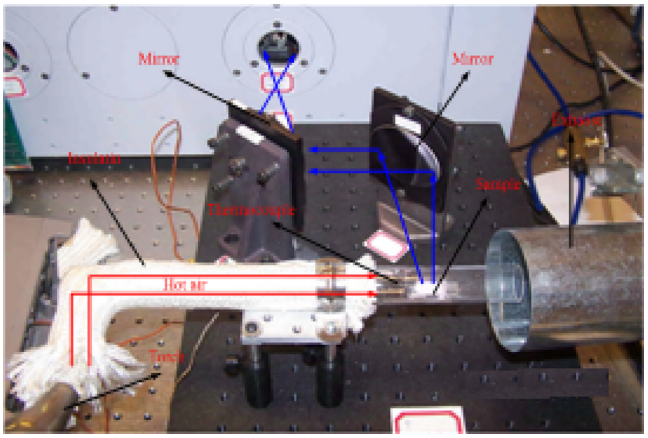

FIG. 8. (Color online) Experimental setup.

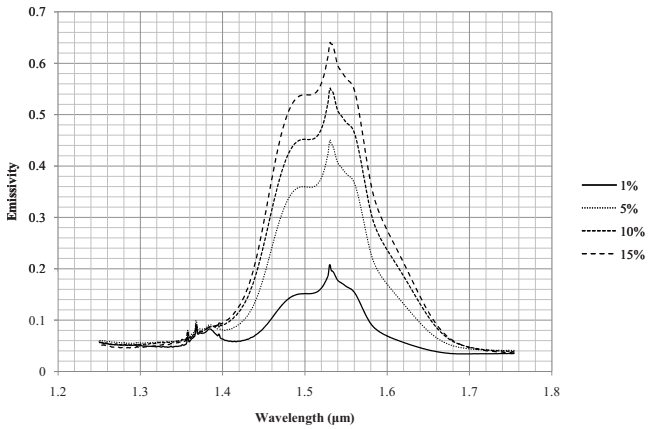

FIG. 9. Measured emissivity of erbia doped alumina fibers at 773 K for different erbium oxide concentration (Er/Al atomic ratio).

a parabolic mirror which collects the radiation emitted from the sample and reflects it to another mirror which reflects it again inside the IR-spectrometer where it is measured and recorded.

To measure the emissivity, a background spectrum is first obtained using a stainless steel fiber sample that has the same dimensions as the prepared selective emitter samples. After that, the sample spectrum is measured at the same temperature. The results for the NIR range are shown in Fig. 9. An emissivity of about 0.65 is achieved for a 15% erbium/aluminum atomic ratio. Increasing the concentration of erbia increased the emissivity of the samples in a nearly linear trend which indicates that there is little or no precipitation of erbia inside the fibers. This is also confirmed in the SEM images taken for the fibers where no clustering of erbia is noticed. Er–Er clustering interaction is believed to be a source of quenching for thermal radiation of erbia.[34]

Figure 10 shows the emissivity at 1.53 μm for erbia doped alumina fiber pellets as a function of pellet thickness. Experimental data for emission is compared to model predictions from Eq. (14). The range of thickness used is from ~190 to 1000 μm. The experimental data shows that as the thickness of the pellet is increasing, emissivity is also increasing to a maximum value. After that, increasing the film thickness induces a very small increase in emissivity. This

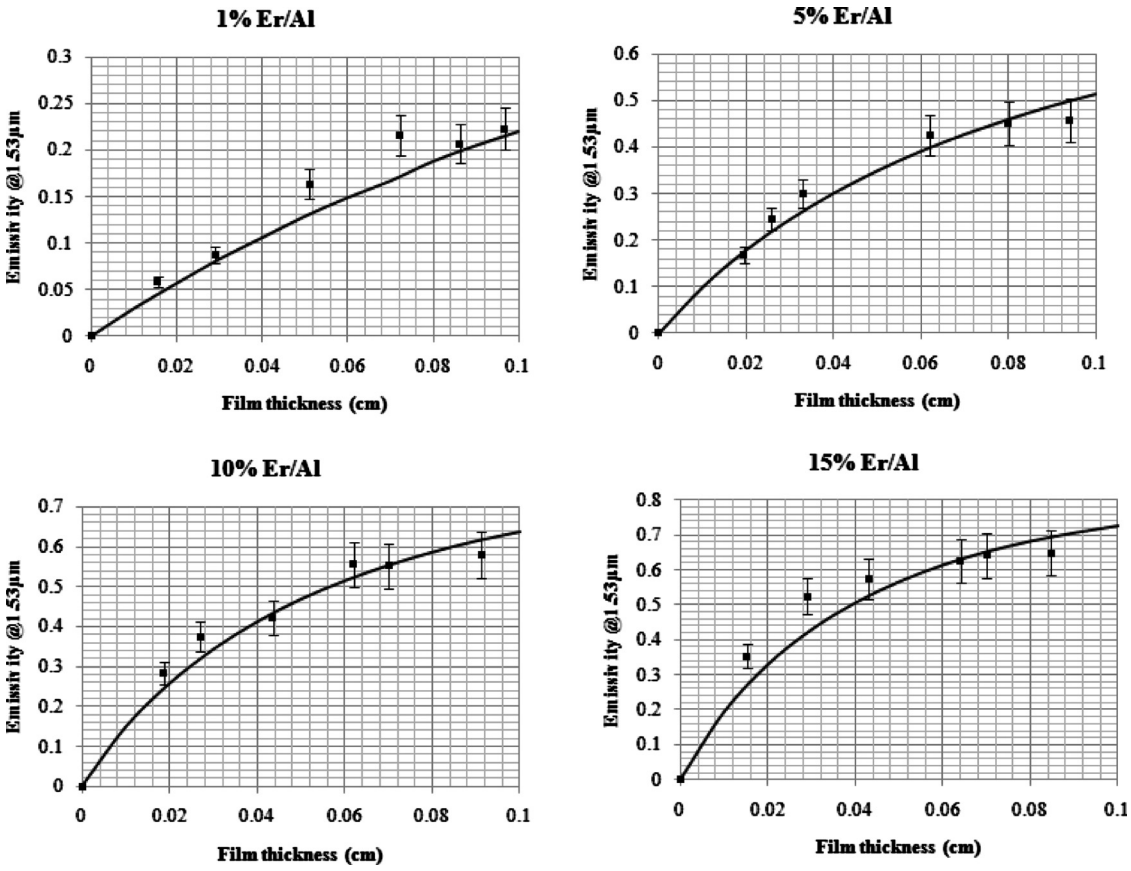

FIG. 10. Comparison of emissivity as a function of film thickness between measured data and model predictions [Eq. (14)]. T=773 K.

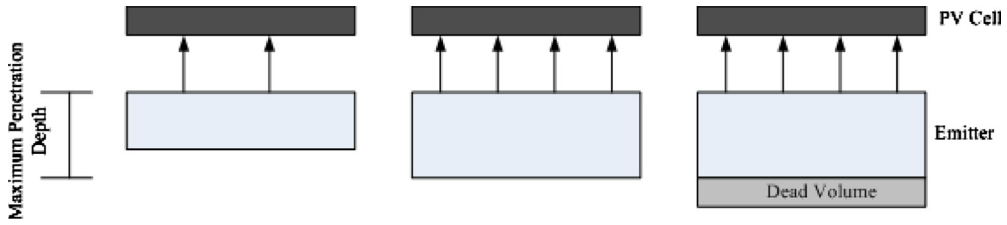

FIG. 11. (Color online) Schematic of maximum penetration depth.

increase indicates that emission is not strictly a surface phenomenon and the emission has contributions from the interior of the pellet.

Depending on film properties such as its porosity, erbia loading level, type of fiber, etc., the film has a certain optical penetration depth. Increasing the film thickness to the maximum penetration depth increases the emissivity of the film because the radiation from the inside of the film can penetrate through the entire thickness of the film and hence be collected at the other end of the sample; however, if the film thickness is larger than the penetration depth, the emissivity does not increase. Radiation energy from the "dead volume" as shown in Fig. 11 is completely depleted due to self-extinction inside the film before it reaches the surface and hence will not be collected. For the samples fabricated here, the maximum penetration depth is approximately 600 μm. The model clearly captured the trend of the emissivity increase with increasing film thickness. Moreover, the agreement between the measured and calculated data is very satisfactory.

Experimental data of radiation energy as a function of wavelength are also compared to calculated data using the model. To calculate the power density, the values of emissivity from Fig. 9 are multiplied by the blackbody radiation intensity at the same temperature calculated from Planck's equation. The result is shown in Fig. 12. The model didn't capture the individual peaks of the erbium oxide because a Gaussian fitting is used to fit the data in Figs. 5 and 6. The benefit of using a selective emitter for TPV applications is shown in this figure by comparing the background radiation from a blackbody emitter and the erbia based selective emitter. The radiation energy emitted from the erbia based emit-

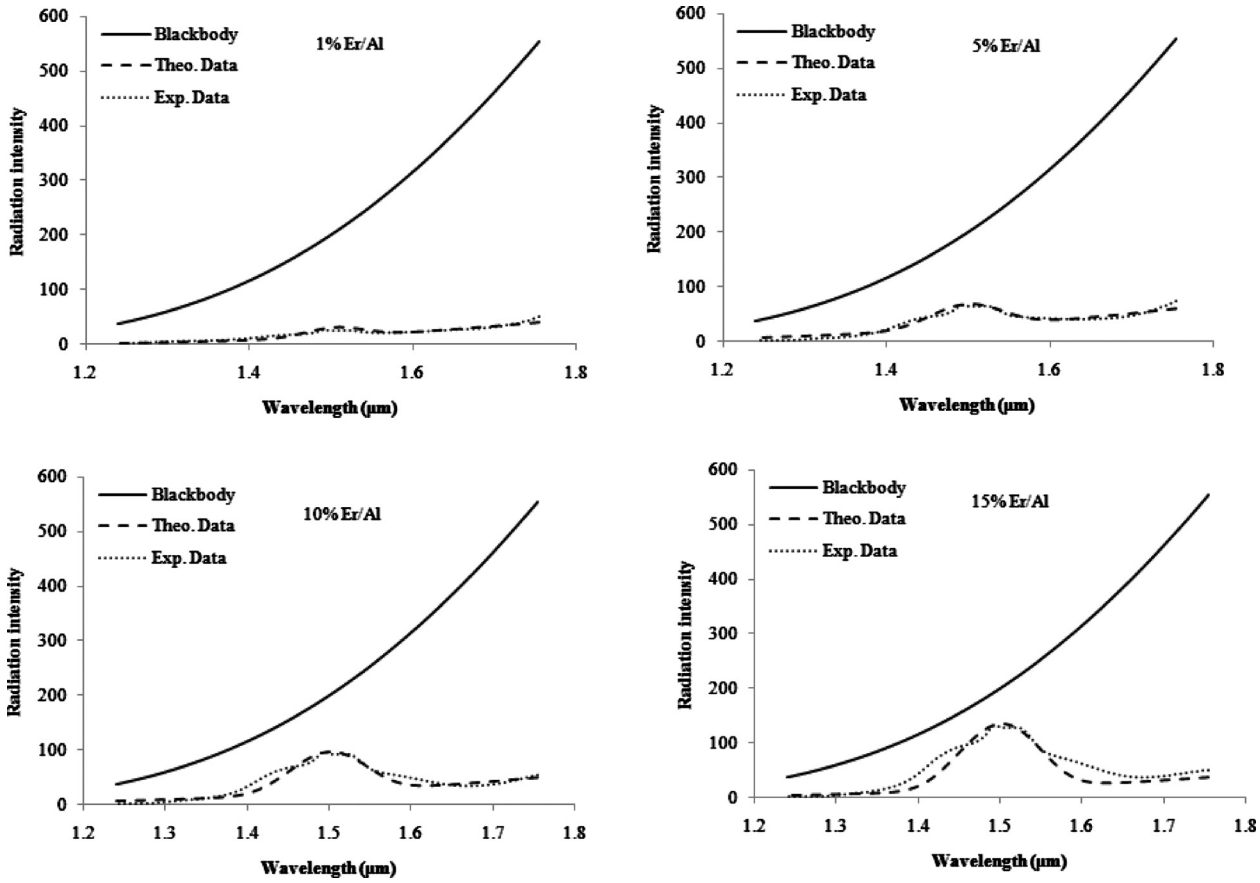

FIG. 12. Comparison of theoretical and experimental data for radiation intensity as a function of wavelength. Substrate emissivity=0, temperature of 773 K, and film thickness=861 cm^{-1}, 800 cm^{-1}, 700 cm^{-1}, and 700 cm^{-1} for the 1%, 5%, 10%, and 15% Er/Al samples, respectively.

TABLE I. PV cells with their corresponding band gap energies and optimum temperature.

Cell type	E_g (eV)	$\lambda_{\_max}$ (μm)	T (K)
Silicon[a]	1.12	1.11	2617
GaSb[a]	0.72	1.72	1682
GaAs	1.42	8.73	3319
Ge[b]	0.67	1.85	1566
InAs[a]	0.36	3.44	841
InGaAs/InP[c]	0.6	2.07	1402
GaInSbAs/GaSb[d]	0.55	2.25	1285

[a]Reference 3.
[b]Reference 35.
[c]Reference 36.
[d]Reference 5.

ters is concentrated in a narrow wavelength range where the radiation from the blackbody is a broad spectrum with a very large amount of off-band radiation.

Having a model that captures the behavior of our nanofiber based selective emitters, we can now study the parameters that affect the emissivity and suggest structures that can improve efficiency.

E. Efficiency analysis

The efficiency of the film can be defined as

$$\varsigma = \frac{\int_0^{\lambda_{bg}} \varepsilon(\lambda)^* e_{BB}(\lambda,T)d\lambda}{\int_0^{\infty} \varepsilon(\lambda)^* e_{BB}(\lambda,T)d\lambda}, \tag{28}$$

where λ_{bg} is the wavelength corresponding to the band gap energy of the PV cell that is being used. Different types of PV cells have different band gap energy. Some common types of PV cells are given in Table I. PV cells operate at maximum efficiency when coupled with photons that have energy equal to their band gap energy.[18] For a blackbody emitter, as the temperature increases, the peak of radiation is shifted to higher radiation intensity and shorter wavelengths as shown in Fig. 13. This means that in order to increase the efficiency of the TPV system, either an emitter with high temperature or a PV cell with low band gap energy is needed. For example, in order to match the maximum energy wavelength of a blackbody emitter with a Si PV cell, the temperature of the emitter has to be 2617 K whereas this temperature is 1682 K for GaSb PV cell.

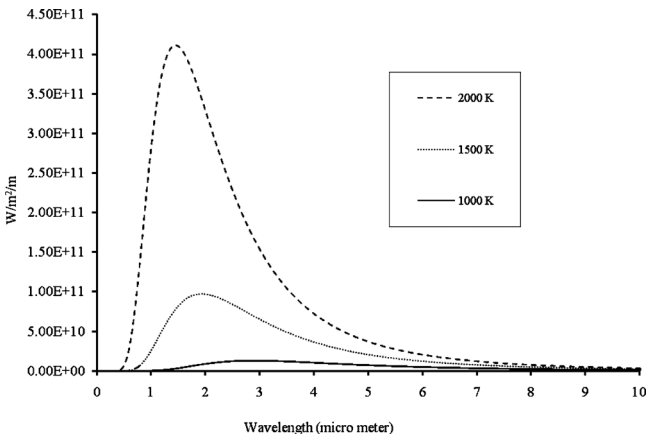

FIG. 13. Blackbody radiation at 1000, 1500, and 2000 K.

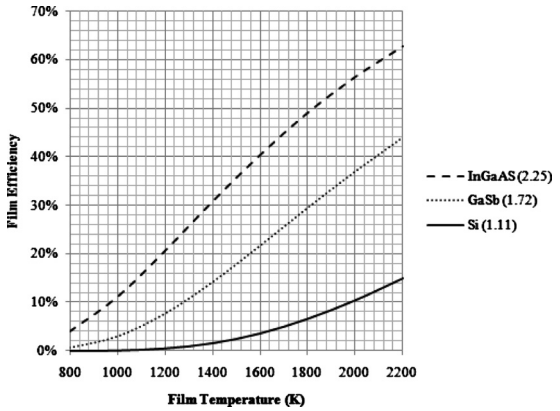

FIG. 14. Film Efficiency as function of temperature for extinction coefficient=10 cm^{-1} and film thickness=0.05 cm.

Controlling the spectral match between the emitter and the PV cell by increasing temperature is an option that is obviously limited by the thermal and the mechanical properties of the emitter material such as its melting point, resistance to oxidation, and thermal shock. Furthermore, increasing the temperature of the emitter means the need for a more efficient and higher capacity cooling system especially if we take into account the sensitivity of PV cells to heat both from a material property and thermodynamic point of view. Obviously, the need for low band gap PV cells is essential to develop an efficient TPV electric generator.

The efficiency of a planar layer as defined in Eq. (28) is shown in Fig. 14 for different types of PV cells. Calculations are made for a thin film with constant extinction coefficient of 10 cm^{-1}. It is clear that increasing the temperature of the emitter increases its efficiency. As the temperature of the emitter is increased, its radiation spectrum is shifted to a shorter wavelength range which means more photons have energy higher than the band gap of the PV cell.

Figure 15 shows the efficiency as a function of film thickness. Increasing the film thickness increases its efficiency because the total emittance of the film is increased. For the different types of PV cells, the trend of efficiency is the same. Further, PV cells with lower band gap energies have higher efficiency.

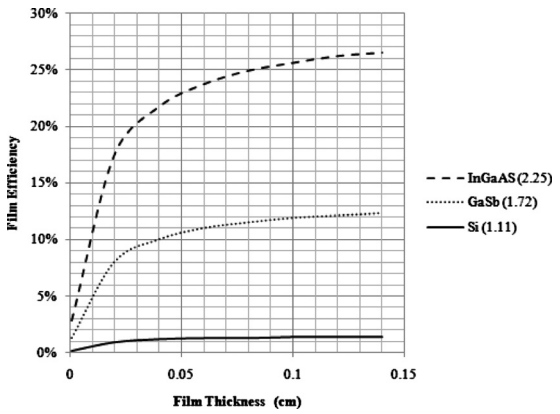

FIG. 15. Efficiency of film thickness as a function of thickness. T =1400 K, extinction coefficient=5 cm^{-1}.

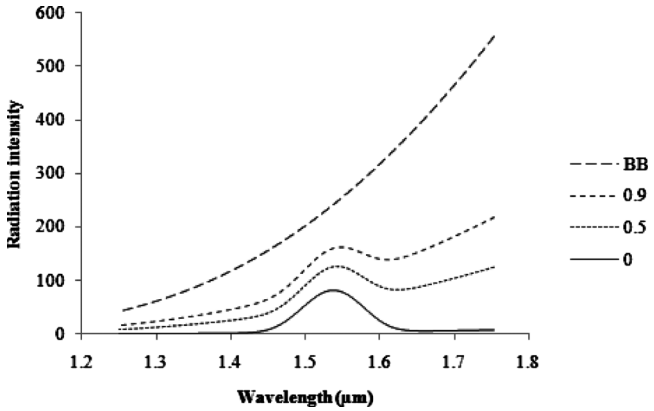

FIG. 16. Effect of substrate emissivity on total power radiated from a thin film selective emitter at 773 K. Substrate emissivity 0, 0.5, and 0.9. BB stands for blackbody radiation at the same temperature.

F. Effect of substrate emissivity

Substrates are often used as a mechanical support for the emitting material. In the 1D model introduced above, the emissivity of the substrate influences the boundary condition at the film/substrate interface and the amount of long wavelength radiation that cannot be converted into electric power in the PV cell. The effect of the substrate emissivity is shown in Fig. 16. Increasing the substrate emissivity increased the total power radiated from the sample; however, the background radiation (radiation that cannot be converted into electricity in the PV cell) from the film increased as well which will decrease the efficiency of the selective emitter.

Clearly from the Fig. 16, low substrate emissivties are needed to attain a high efficiency. The effect of the substrate emissivity can be reduced by controlling the thickness of the film. In the cases where a substrate is needed to improve the mechanical durability of the emitter, if the thickness of the film is larger than its maximum optical penetration depth, the radiation from the substrate cannot penetrate the film and, therefore, will not reach the PV cell. This principle is demonstrated in Fig. 17. The emissivity of a stainless steel substrate is first measured and then a layer of erbia doped titania nanofibers is pressed on top of it and the emissivity is measured again. The off-band radiation from the substrate is greatly reduced. However, using films with very large thickness may result in larger temperature gradients inside the film which reduces the radiated power from the film. As a result using a substrate is subject to many factors that include the type of materials used, geometry of the emitter, desired mechanical properties, and the operating temperatures which can be optimized by calculating the efficiency of the emitter.

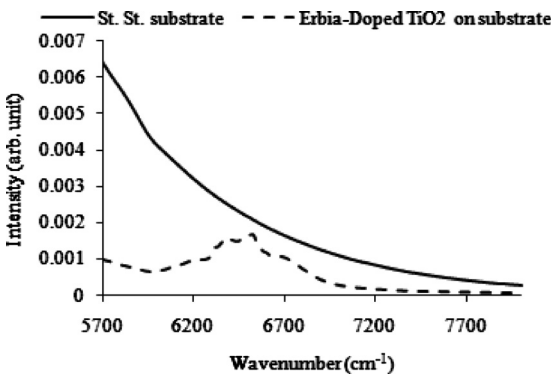

FIG. 17. Experimental measurements of radiation intensity of an erbia doped titanium oxide thin film supported on a blackbody substrate. Fiber film thickness=0.1 cm. Temperature=773 K.

V. CONCLUSIONS

Selective emitters based on erbia doped ceramic nanofibers are fabricated using the electrospinning technique. It is found that an emissivity of about 0.65 is achievable for emitters that have 15% Er/Al atomic ratio. The general equation of radiation transfer coupled with experimentally measured optical properties is effectively used to predict the net radiation from the fabricated structures. After experimentally validating the model, it is used to study the effect of film thickness, extinction coefficient, and substrate emissivity on the overall emissivity in order to suggest structures for efficient TPV emitters. Substrates with high emissivity decrease the efficiency of the selective emitter by increasing the off-band radiation from the emitter. This effect is overcome by using free-standing emitters made of electrospun fibers. Controlling the thickness of the emitting material may also be used in principle to suppress the substrate emissivity.

ACKNOWLEDGMENTS

The authors would like to acknowledge Professor Sasa Dordevic for his help with the IR analysis. This work was supported by NSF Grant No. DMI-0403835.

[1]A. Licciulli, A. Maffezzoli, D. Diso, S. Tundo, M. Rella, G. Torsello, and M. Mazzer, J. Sol-Gel Sci. Technol. **26**, 1119 (2003).
[2]T. J. Coutts, Renewable Sustainable Energy Rev. **3**, 77 (1999).
[3]S. Basu, Y.-B. Chen, and Z. M. Zhang, Int. J. Energy Res. **31**, 689 (2007).
[4]E. Guido Guazzoni, Appl. Spectrosc. **26**, 1 (1972).
[5]A. Licciulli, D. Diso, G. Torsello, S. Tundo, A. Maffezzoli, M. Lomascolo, and M. Mazzer, Semicond. Sci. Technol. **18**, S174 (2003).
[6]D. Diso, A. Licciulli, A. Bianco, M. Lomascolo, G. Leo, M. Mazzer, S. Tundo, G. Torsello, and A. Maffezzoli, Mater. Sci. Eng., B **98**, 144 (2003).
[7]S.-C. Lee and G. R. Cunnington, J. Thermophys. Heat Transfer **14**, 121 (2000).
[8]E. T. Bender, R. Wang, M. T. Aljarrah, E. A. Evans, and R. D. Ramsier, J. Vac. Sci. Technol. A **25**, 922 (2007).
[9]R. Wang, E. T. Bender, M. T. Aljarrah, E. A. Evans, and R. D. Ramsier, MRS Symposia Proceedings No. 957 (Materials Research Society, Pittsburgh, 2007), p. 1023-JJ05-07.
[10]S.-C. Lee and G. R. Cunnington, Jr., Annu. Rev. Heat Transfer **9**, 159 (1998).
[11]D. L. Chubb and R. A. Lowe, J. Appl. Phys. **74**, 5687 (1993).
[12]D. L. Chubb, B. S. Good, E. B. Clark, and Z. Chen, NASA Lewis Research Center, Report No. NASA/TM-107523, 1997.
[13]R. A. Lowe, D. L. Chubb, S. C. Farmer, and B. S. Good, Appl. Phys. Lett. **64**, 26 (1994).
[14]R. Siegel and J. R. Howell, *Thermal Radiation Heat Transfer*, 3rd ed. (McGraw-Hill, New York, 1992).
[15]D. L. Chubb, R. A. Lowe, and B. S. Good, Report No. NASA/TM 106727, 1994.
[16]*Fifth Conference Thermophotovoltaic Generation of Electricity*, edited by T. J. Couts, G. Guazzoni, and J. Luther (American Institute of Physics, Melville, 2003), p. 0-7354-0113-6.
[17]M. F. Modest, *Radiative Heat Transfer* (McGraw-Hill, New York, 1993).
[18]D. L. Chubb, *Fundamentals of Thermophotovoltaic Energy Conversion*, 1st ed. (McGraw-Hill, Columbus, OH, 2007).
[19]R. Siegel and J. R. Howell, *Thermal Radiation Heat Transfer*, 3rd ed. (Elsevier, Amsterdam, 1992).

[20]D. L. Chubb, A. M. T. Pal, M. O. Patton, and P. P. Jenkins, Report No. NASA/TM-208835, 1999.
[21]D. L. Chubb, Report No. NASA/TM-208656, 1998.
[22]D. L. Chubb, A. M. T. Pal, M. O. Patton, and P. P. Jenkins, J. Eur. Ceram. Soc. **19**, 2551 (1999).
[23]Y. M. Shin, M. M. Hohman, M. P. Brenner, and G. C. Rutledge, Appl. Phys. Lett. **78**, 1149 (2001).
[24]G. Larsen, R. Velarde-Ortiz, K. Minchow, A. Barrero, and I. G. Loscertales, J. Am. Chem. Soc. **125**, 5 (2003).
[25]W. Kataphinan, R. Teye-Mensah, and E. A. Evans, J. Vac. Sci. Technol. A **21**, 1574 (2003).
[26]A.-M. Azad, Mater. Lett. **60**, 1 (2006).
[27]P. Viswanathamurthi, N. Bhattarai, H. Y. Kim, D. I. Cha, and D. R. Lee, Mater. Lett. **58**, 3368 (2004).
[28]R. Teye-Mensah, V. Tomer, W. Kataphinan, J. C. Tokash, N. Stojilovic, G. G. Chase, E. A. Evans, R. D. Ramsier, D. J. Smith, and D. H. Reneker, J. Phys.: Condens. Matter **16**, 7557 (2004).
[29]W. Sigmund, J. Yuh, H. Park, V. Maneeratana, G. Pyrgiotakis, A. Daga, J. Taylor, and J. C. Nino, J. Am. Ceram. Soc. **89**, 395 (2006).
[30]M. T. Aljarrah, E. A. Evans, J. Hicks, C. B. Clemons, and G. W. Young, J. Appl. Phys. **109**, 034307 (2011).
[31]Y. Liu, J.-H. He, Y. Jian-yong, and Z. Hong-mei, Polym. Int. **57**, 4 (2008).
[32]S. Tripatanasuwan, Z. Zhong, and D. H. Reneker, Polymer **48**, 5742 (2007).
[33]M. Ghanashyam Krishna, R. G. Biswas, and A. K. Bhattacharya, J. Phys. D: Appl. Phys. **30**, 8 (1997).
[34]J. Wu and J. L. Coffer, Chem. Mater. **19**, 25 (2007).
[35]A. Catalano, WREC-IV World Renewable Energy Congress No 4, ETATS-UNIS, Denver, Colorado, 15 June 1996,Vol. 8, pp. 495–499.
[36]L. M. Fraas, J. E. Avery, H. X. Huang, and R. U. Martinelli, Semicond. Sci. Technol. **18**, 5 (2003).